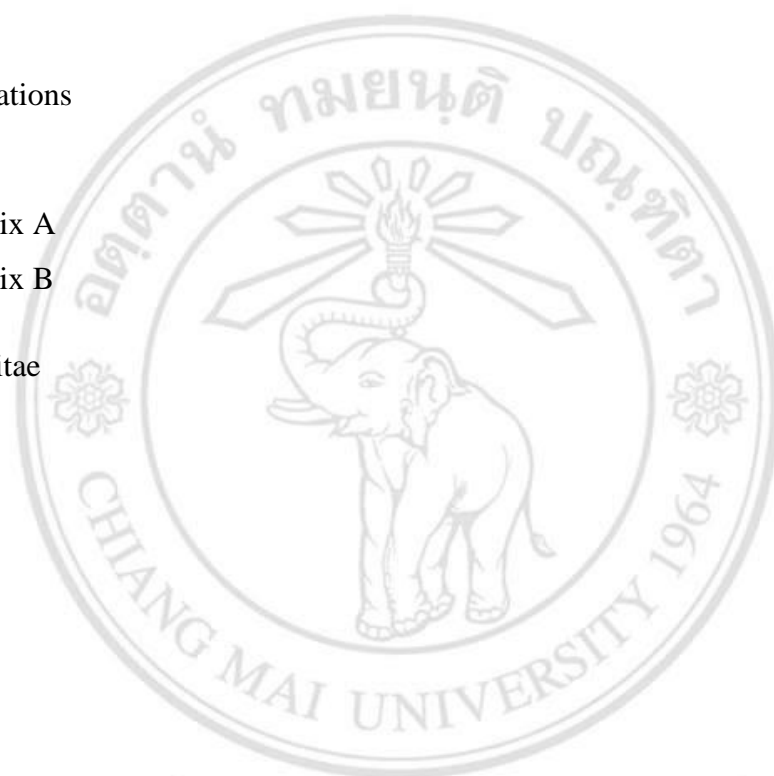


# CONTENTS

	Page
Acknowledgement	c
Abstract in English Thai	e
Abstract in English	g
List of Tables	k
List of Figures	l
Statement of Originality in Thai	r
Statement of Originality in English	s
Chapter 1 Introduction	1
1.1 Research Overviews	1
1.2 Research objectives	3
Chapter 2 Theoretical background	4
2.1 Electrochemical energy storage	4
2.2 Batteries	42
2.3 Sparking method	46
2.4 Characterization techniques	47
Chapter 3 Experiment	65
3.1 Experimental equipment	65
3.2 Experimental procedure	67
3.3 Material characterizations	70
3.4 Electrochemical measurement	77
Chapter 4 Results and Discussion	79
4.1 Results and discussion of the NiO films sparked on flexible Cr/Au coated PET substrates	79

4.2 Results and discussion of the NiO film on Ni foams	92
Chapter 5 Conclusions and Suggestions	110
5.1 The NiO films sparked on flexible PET coated Cr/Au substrates	110
5.2 The NiO film on Ni foams	110
5.3 Suggestions for future work	111
References	112
List of publications	136
Appendices	137
Appendix A	138
Appendix B	147
Curriculum vitae	160



ลิขสิทธิ์มหาวิทยาลัยเชียงใหม่  
 Copyright© by Chiang Mai University  
 All rights reserved

## LIST OF TABLES

	Page
Table 2.1 Some properties of some commercial microporous membranes separators Table 2.1	19
Table 2.2. The specific capacitance relate to the electrolytes materials	20
Table 2.3. Summarized the synthesis method and electrochemical performance of some polymer (PPy, PT and PANi) based on pseudocapacitor electrode	41
Table 4.1 Charge storage performances of NiO-based electrodes prepared by various methods	107

## LIST OF FIGURES

	Page
Figure 2.1 Schematic diagram of a supercapacitor device	5
Figure 2.2. Models of the electrical double layer	6
Figure 2.3. The construction of (a) conventional capacitors and (b) EDLCs capacitors	8
Figure 2.4. The rectangular i-V curve with the variation of the scan rates for $C = 50 \text{ mF}$ , $V_{\text{max}} = 5 \text{ V}$	10
Figure 2.5. Schematic representation of GCD graph at constant currents as achieved from equation 2.5	10
Figure 2.6. The charge storage procedure in a pseudo-capacitive material	12
Figure 2.7. (a) CV pattern at a various scan rate and (b) GCD graph with a different charged/discharged current of an assumed positive battery electrode	14
Figure 2.8. The band theory and its deal with conductivity, charge storage performance and pattern of insulators, semiconductors and metals	15
Figure 2.9. The schematic illustration of RC circuit	17
Figure 2.10. CV pattern of activated glassy carbon electrodes in $3\text{M H}_2\text{SO}_4$ aqueous electrolyte and in $1 \text{ M TEABF}_4$ in acetonitrile at the scan rate of $100 \text{ mV/s}$	21
Figure 2.11. Ragone plot presenting energy density against power density of the various energy storage devices	22
Figure 2.12. The group of supercapacitors and its electrode materials used	23
Figure 2.13. The specific capacitance normalized by specific surface area vs. average pore size of various carbon samples	24
Figure 2.14. The SEM of random distribution SWCNTs	26
Figure 2.15. The SEM pictures of (a) the as-grown forest SWCNT (b) SECNT after liquid-induced densification process	26

Figure 2.16. A Schematic showing of the plasma-etched VA-CNTs used as supercapacitor electrode in an ionic liquid electrolyte (IL)	27
Figure 2.17. (a-b) low and high magnification SEM images of the plasma-etched VA-CNTs (c-d) TEM images of the sample before and after plasma etching	28
Figure 2.18. The Schematic diagram of the method of laser-scribed graphene (LSG) based on supercapacitor	29
Figure 2.19. (a) Schematic diagram of the flexible supercapacitor based on LSG. (b) The performance of LSG-EC between a gelled electrolyte vs. an aqueous electrolyte. (c) The CV shape of the Flexible LSG-EC@ 1000 mV s <sup>-1</sup>	29
Figure 2.20. The performance of an LSG supercapacitors in 1.0 M H <sub>3</sub> PO <sub>4</sub> electrolyte	30
Figure 2.21. The CV pattern of MnO <sub>2</sub> at scan rate of 2,10,20 mV s <sup>-1</sup>	32
Figure 2.22. The cubic NiO structure	33
Figure 2.23. The SEM images of (a) NiO nanoflower, (b) NiO nanoslice, (c) NiO nanoparticle synthesized via Sol-Gel method and (d) the comparison of CV graph of three different shaped NiO at 50 mV/s	35
Figure 2.24. (a)-(b) the SEM pictures at low and high magnification, (c) CV curves at different scan rates and (d) GCD curves at various current densities of NiO network-like hierarchical microspheres by ultrathin nanowires self-assembly electrode	35
Figure 2.25. (a) SEM image, (b) different TEM image, (c) the specific capacitance retention at different current densities and (d) cycle performance at the current density of 2 A g <sup>-1</sup> of the mesoporous NiO electrode	36
Figure 2.26. (a) SEM image, (b) high-resolution TEM image and (c) CV graph at various scan rate of the NiO with mesoporous structure, prepared by the template method	36
Figure 2.27. (a)-(b) SEM image at low and high magnifications, (c) GCD graph at various current densities and (d) the cycling capabilities	

	at a current density of $3 \text{ A g}^{-1}$ (The inset depicted the first 10 cycle of the test.) of the NiO of the nanospherical porous NiO electrode	37
Figure 2.28.	(a) SEM image of NiO prepared by reflux approach (NiO-ref), (b) SEM image of NiO prepared by microwave assisted heating technique (NiO-mw), (c) the comparison of GCD plot at various current densities vs cycle number of NiO-ref and NiO-mw electrode	38
Figure 2.29.	(a) SEM image of ultrafine $\text{Co}_3\text{O}_4$ , (b) CV patterns of samples A=Co-P123-PH3, B=Co-P123 and C=Co-CA at the scan rate of $5 \text{ mV s}^{-1}$ , (c) the specific capacitance vs. current densities and (d) the relationship between the average specific capacitance and cycling number of Co-P123-PH3 at $20 \text{ mV s}^{-1}$	39
Figure 2.30.	Various structures of conducting polymers	40
Figure 2.31.	The schematic illustration of the comparison of the volumetric and gravimetric energy densities of various batteries	42
Figure 2.32.	The Pb-acid battery working mechanism	43
Figure 2.33.	The construction of Ni-Cd battery (a) the cylindrical cell and (b) the prismatic cell	44
Figure 2.34.	The construction of Ni-Mh battery (a) the prismatic cell and (b) the cylindrical cell	45
Figure 2.35.	The nucleation mechanism of the sparked products such as transition metal oxide thick/thin films or nanoparticles	46
Figure 2.36.	Various interactions of an incident electron beam with a solid material	47
Figure 2.37.	The main components of a scanning electron microscope	51
Figure 2.38.	Ray paths in a reference transmission electron microscope (a) Bright field imaging mode, (b) Selected area diffraction mode	53
Figure 2.39.	The diffraction of X-rays by planes of atoms ( $A - A'$ and $B - B'$ )	54
Figure 2.40.	Schematic diagram of 2p photoelectron is emitted from copper and accompanies excitation of the atom by absorption of an X-ray photon	56
Figure 2.41.	Energy diagram of light-induced excitation	57
Figure 2.42	Light absorbed by the sample in a cuvette	58
Figure 2.43	The basic working diagram of the AFM	61

Figure 2.44 The IUPAC classification of adsorption isotherms	62
Figure 2.45 BET plot displays a linear feature	63
Figure 3.1. Schematic illustration of the sparking system for fabrication of NiO films	68
Figure 3.2. A diagram strategy of NiO film on flexible PET coated Cr/Au substrates for electrochemical test	68
Figure 3.3. A diagram strategy of NiO film on Nickel foam for electrochemical test	69
Figure 3.4 Field Emission Scanning Electron Microscope (FE-SEM, JEOL JSM-6335F) including Energy Dispersive X-ray Spectroscopy (EDS)	71
Figure 3.5 Field Emission Scanning Electron Microscope (FE-SEM, Hitachi model SU-8030) equip with Energy Dispersive X-ray Spectroscopy (EDS)	71
Figure 3.6 Transmission Electron Microscope (TEM, JEOL JEM-2010)	72
Figure 3.7 Raman spectrophotometer (Renishaw model Invia) operated with an argon ion laser	73
Figure 3.8 the Atomic Force Microscope ( <u>Nano Scope IIIa</u> , Digital Instruments)	73
Figure 3.9 UV-vis spectrophotometer (Varian Cary 50, U.S.A)	74
Figure 3.10 Brunauer-Emmett-Teller (Autosorb 1 MP, Quantachrome, USA)	75
Figure 3.11 X-ray diffraction (GIXRD, Rigaku Ttrax III)	76
Figure 3.12 X-ray photoelectron spectroscopy (AXIS Ultra DLD, England)	76
Figure 3.13. The $\mu$ -Autolab Type III electrochemical work station (ECO-Chemie, Metrohm, Switzerland)	77
Figure 3.14. The Autolab PGSTAT302N (ECO-Chemie, Metrohm, Switzerland)	77
Figure 3.15. The schematic depicting of the 3-electrodes configuration for electrochemical test	78
Figure 4.1 The SEM images of the sparked NiO film: top-view at (a) low and (b) high magnifications and (c) cross-sectional-view	80
Figure 4.2 (a) 2D, (b) 3D AFM topographic images of Cr-Au on PET substrate, (c) 2D and (d) 3D AFM topographic images of NiO sparked surfaces	81
Figure 4.3 (a) TEM image, (b) HR-TEM image, (c) SAED pattern and (d) EDX	

spectrum of sparked NiO-NPs	82
Figure 4.4 Nitrogen adsorption and desorption isotherms of NiO film	83
Figure 4.5 The corresponding BJH pore size distribution of NiO film	83
Figure 4.6 GIXRD pattern of sparked NiO film on Au/Cr coated PET substrate	84
Figure 4.7 UV-vis spectrum (Inset: plot of $(\alpha hv)^2$ vs. $h\nu$ )	85
Figure 4.8 (a) Ni 2p and (b) O 1s XPS spectra of sparked NiO film	86
Figure 4.9 (a) CV curve of the Cr-Au on PET substrate vs. sparked NiO film at a scan rate of $10 \text{ mV s}^{-1}$ , (b) CV graph of NiO film at different scan rates and (c) oxidation peak current vs. square root of scan rate of sparked NiO film	88
Figure 4.10 (a-b) GCD data of NiO films at low and high ranges of discharge current density, (c) specific capacity curves at a variety of current densities (Inset: photograph of bent electrode before testing)	89
Figure 4.11 (a) GCD profiles of repeated 10 cycles at $40 \text{ A g}^{-1}$ and (b) cycling performance of sparked NiO films at $40 \text{ A g}^{-1}$	91
Figure. 4.12 SEM images of (a) Ni foam, (b) NiO-45min, (c) NiO-90min, (d) NiO-135min and (e) NiO-180min	93
Figure. 4.13 The corresponding EDX spectra of (a) Ni foam, (b) NiO-45min, (c) NiO-90 min (d) NiO-135min, and (e) NiO-180min	95
Figure. 4.14 TEM images and corresponding SAED patterns of NiO nanoparticles produced at sparking times of (a) 45 and (b) 180 min	96
Figure 4.15 Raman spectra of sparked NiO nanoparticles on Ni foams with different sparking times	97
Figure 4.16 XPS spectra of NiO nanoparticles on Ni foams produced at sparking times of 45 and 180 min: (a) survey scan, (b) Ni 2p and (c) O 1s	98
Figure 4.17 CV curves at various scan rates of NiO/Ni foam electrodes prepared with the sparking times of (a) 45 min, (b) 90 min, (c) 135 min and (d) 180 min, (e) corresponding anodic peak current vs. the square root of scan rate plots and (f) corresponding specific capacity vs. scan rate plots	101
Figure 4.18 GCD curves at various current densities of NiO/Ni foam electrodes	

prepared with the sparking times of (a) 45 min, (b) 90 min,  
(c) 135 min and (d) 180 min, (e) GCD curves at a current density of  
1 A g<sup>-1</sup> of sparked NiO films with varying sparking times and  
(f) the corresponding specific capacity vs. current density

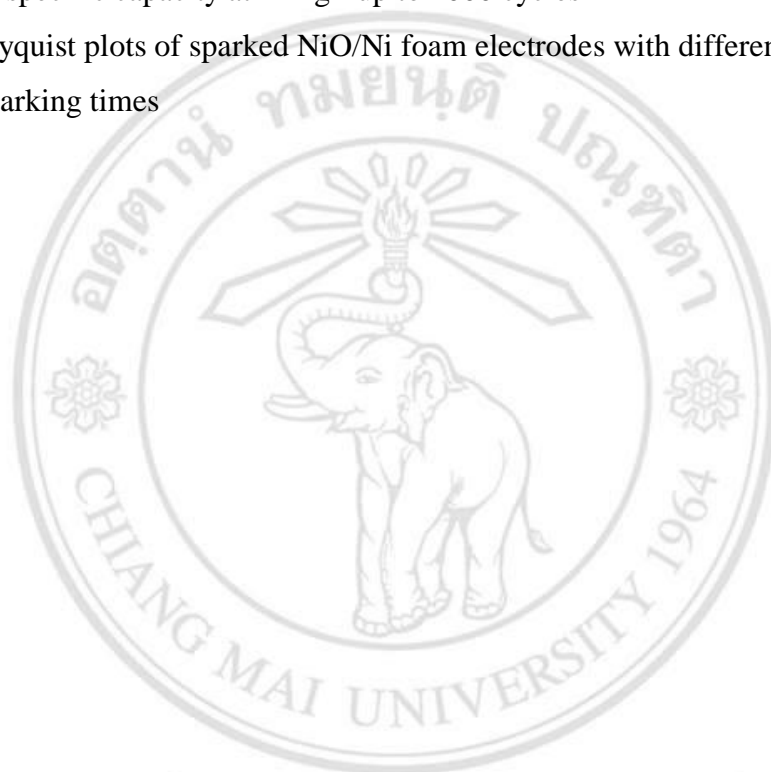
103

Figure 4.19 (a) The first 10 cycles of GCD profiles at 4 A g<sup>-1</sup> of NiO-45min  
and NiO-180min and (b) the corresponding cycling performance  
of specific capacity at 4 A g<sup>-1</sup> up to 1000 cycles

106

Figure 4.20 Nyquist plots of sparked NiO/Ni foam electrodes with different  
sparking times

108



ลิขสิทธิ์มหาวิทยาลัยเชียงใหม่  
Copyright© by Chiang Mai University  
All rights reserved

## STATEMENT OF ORIGINALITY IN THAI

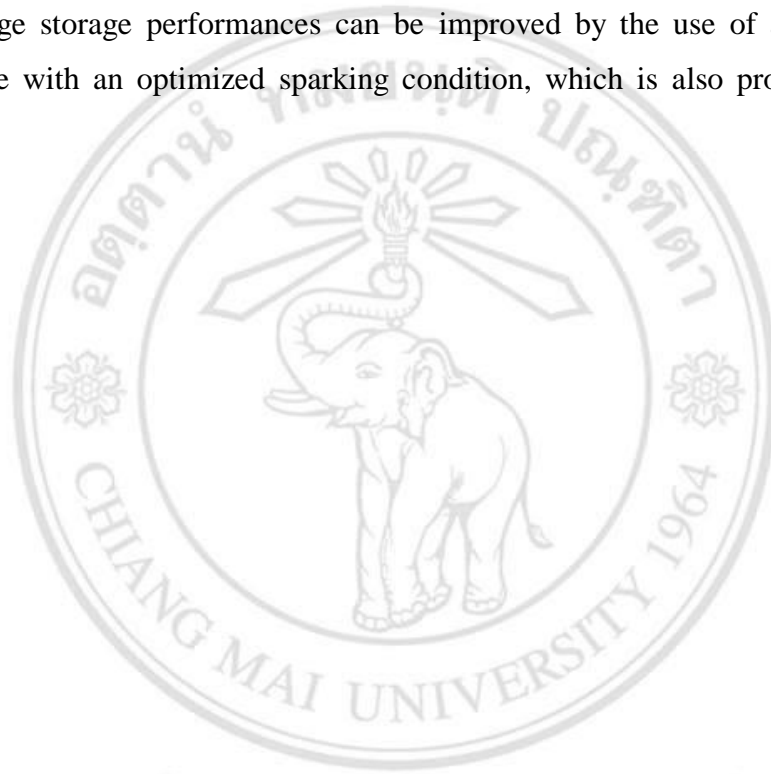
1. วิทยานิพนธ์นี้นำเสนอวิธีการสปาร์คซึ่งเป็นกระบวนการใหม่สำหรับใช้เตรียมอนุภาคนาโนและฟิล์มนิกเกิลออกไซด์เพื่อใช้งานในการกักเก็บพลังงานไฟฟ้าเคมี
2. สามารถเพิ่มสมรรถนะในการกักเก็บประจุได้โดยการใช้ฐานรองที่มีความพรุนสูงและเตรียมด้วยเงื่อนไขในการสปาร์คที่ดีที่สุด ซึ่งได้นำเสนอไว้ในการศึกษาครั้งนี้ด้วย



ลิขสิทธิ์มหาวิทยาลัยเชียงใหม่  
Copyright© by Chiang Mai University  
All rights reserved

## STATEMENT OF ORIGINALITY IN ENGLISH

1. This thesis represents a sparking method, which is a relatively new method for fabrication of nickel oxide nanoparticles and nickel oxide films for battery-type electrochemical energy storage applications.
2. Its charge storage performances can be improved by the use of a high porous substrate with an optimized sparking condition, which is also proposed in this study.



ลิขสิทธิ์มหาวิทยาลัยเชียงใหม่  
Copyright© by Chiang Mai University  
All rights reserved